Journal of Chromatography A, 1218 (2011) 1219–1226

Contents lists available at ScienceDirect

Journal of Chromatography A

journal homepage: www.elsevier.com/locate/chroma

Characterization and modeling of nonlinear hydrophobic interaction chromatographic systems

Deepak Nagrath[a,1], Fang Xia[b,1], Steven M. Cramer[c,*]

[a] Department of Chemical and Biomolecular Engineering, Rice University, TX, USA
[b] Amgen, Thousand Oaks, CA, USA
[c] Department of Chemical and Biological Engineering, Rensselaer Polytechnic Institute, 110, 8th Street, Troy, NY 12180-3590, USA

ARTICLE INFO

Article history:
Received 12 August 2010
Received in revised form
24 December 2010
Accepted 31 December 2010
Available online 6 January 2011

Keywords:
Hydrophobic interaction chromatography
General rate model
Preferential interaction isotherm

ABSTRACT

A general rate model was employed in concert with a preferential interaction quadratic adsorption isotherm for the characterization of HIC resins and the prediction of solute behavior in these separation systems. The results indicate that both pore and surface diffusion play an important role in protein transport in HIC resins. The simulated and experimental solute profiles were compared for two model proteins, lysozyme and lectin, for both displacement and gradient modes of chromatography. Our results indicate that a modeling approach using the generate rate model and preferential interaction isotherm can accurately predict the shock layer response in both gradient and displacement chromatography in HIC systems. While pore and surface diffusion played a major role and were limiting steps for proteins, surface diffusion was seen to play less of a role for the displacer. The results demonstrate that this modeling approach can be employed to describe the behavior of these non-linear HIC systems, which may have implications for the development of more efficient preparative HIC separations.

1. Introduction

Hydrophobic interaction chromatography (HIC) is an entropically driven process that uses the hydrophobic interaction between the hydrophobic resin and non-polar hydrophobic patches on the solute surface to effect the separation. HIC has been shown to have significant utility for the separation of proteins from complex mixtures [1–11]. There have been significant efforts towards understanding the mechanism of protein retention in HIC systems [4,11–27]. The solvophobic theory [12] is based on the association and solvation of the participating species and relates the molal surface tension increment of the salt to retention [14,21,22]. Fausnaugh and Regnier [23] studied the adsorption of several proteins in the presence of different salt types and found that the solvophobic theory alone could not adequately explain retention differences. The preferential interaction theory [15] has been shown to successfully capture salt type effects [18,25] and has been applied to study solute binding and selectivity [26] as well as the effects of pH in HIC systems at low column loadings [24]. A preferential interaction quadratic (PIQ) adsorption isotherm model has also been developed that can describe the effect of salt on both the linear and the nonlinear adsorption of proteins and small molecules in HIC systems [28]. Recently, a new thermodynamic isotherm has been proposed that describes adsorption in terms of water displacement, protein and ligand density and distinguishes the effects of ligand densities and types [29–30]. Furthermore, Lienqueo et al. [31] have recently developed a methodology for optimizing performance of protein mixtures in HIC systems using simple rate model.

The general rate model of chromatography is the most comprehensive of all the transport models and has been used to describe both linear [32,33] and nonlinear [34–36] chromatographic systems. The general rate model developed by Berninger et al. [34] includes the possibility of reactions in the mobile and stationary phases. On the other hand, the general rate model presented by Ma et al. [35] encompasses a generalized parallel (pore and surface diffusion) model for multicomponent adsorption [37]. Previously, we [38] have developed a general rate model based on nonequilibrium steric mass action kinetics for ion-exchange separations.

In order to characterize a given chromatographic system, it is useful to determine the relative importance of various transport and kinetic effects. Wang et al. examined various rate-limiting steps in chromatographic systems and derived solute moment profiles for these types of mechanisms [34,35,39,40]. Work has also been carried out to determine the controlling mechanisms in IEX systems [41,42]. Natarajan and Cramer [43] presented a methodology to compare the relative importance of IEX resin transport parameters and to select appropriate transport models.

* Corresponding author. Tel.: +1 518 276 6198; fax: +1 518 276 4030.
E-mail addresses: crames@rpi.edu, swcchung@gmail.com (S.M. Cramer).
[1] Both authors equally contributed.

0021-9673/$ – see front matter © 2011 Elsevier B.V. All rights reserved.
doi:10.1016/j.chroma.2010.12.111

In the present paper, we present a general rate model for characterizing HIC systems and for predicting both displacement and gradient protein separations. Equations relating the second moment variance to flow rate and retention are developed. A methodology is then presented to estimate the transport and kinetic parameters using data obtained from pulse injections under retained and unretained conditions. Dimensionless groups are then calculated to evaluate the relative contributions of the different transport mechanisms. Finally, the general rate model is coupled with the preferential interaction quadratic isotherm for the prediction of nonlinear chromatographic behavior in HIC column systems.

2. Theory

2.1. Preferential interaction quadratic (PIQ) isotherm

The PIQ isotherm is capable of predicting solute adsorption behavior under both linear and nonlinear conditions over a wide range of salt concentrations [28] and is given by the following:

$$Q_i = \frac{k_i' \cdot (a_i \cdot C_i + d_i \cdot C_i^2)}{1 + \sum_{j=1}^{N_c} k_j' \cdot (b_j \cdot C_j + c_j C_j^2)} \tag{1}$$

$$\ln k_i' = \alpha_i + \beta_i \cdot C_{\text{salt}} + \gamma_i \cdot \ln(C_{\text{salt}}) \tag{2}$$

where i and j denote solutes; C_i and Q_i are concentrations in the liquid and solid phases respectively; k' is the capacity factor; N_c is the number of components; and C_{salt} is the salt (modulator) concentration. α, β and γ are the retention parameters that are determined from isocratic experiments under linear adsorption conditions. a, b, c and d are the isotherm parameters that are obtained by fitting the isotherms under a range of conditions. The equilibrium constant for the above equations is given by

$$K_i = k_i' \cdot a_i = a_i \cdot \exp(\alpha_i + \beta_i C_{\text{salt}} + \gamma_i \ln(C_{\text{salt}})) \tag{3}$$

2.2. Mass transport equations

In the general rate model, the mass balance equation for a given solute in the mobile phase can be written as:

$$\frac{\partial C_i}{\partial t} = D_{ai}\frac{\partial^2 C_i}{\partial x^2} - u_o\frac{\partial C_i}{\partial x} - \frac{(1-\varepsilon_i)}{\varepsilon_i}\frac{3k_{fi}}{R}[C_i - C_{pi}(r=R)] \tag{4}$$

where the initial and boundary conditions are:

$$C_i = C_i(0,x), \quad i = 1, 2, \ldots N \tag{5}$$

$$E_i\frac{\partial C_i}{\partial x} = \begin{cases} 0 & x = L \\ u_0[C_i - C_{fi}(t)] & x = 0 \end{cases}, \quad i = 1, 2, \ldots N \tag{6}$$

The mass balance of the solute inside the pores of the resin is given by:

$$\frac{\varepsilon_p \partial[C_{p,i}]}{\partial t} + \frac{(1-\varepsilon_p)\partial[Q_i]}{\partial t} = \varepsilon_p D_{ap,i}\frac{1}{r^2}\frac{\partial[r^2(\partial C_{p,i}/\partial r)]}{\partial r} \tag{7}$$

With initial and boundary conditions as:

$$C_{pi} = C_{pi}(0,r) \tag{8}$$

$$\varepsilon_p D_{api}\frac{\partial C_{p,i}}{\partial r} = k_{f,i}(C_i - C_{p,i}), \quad r = R \tag{9}$$

$$\frac{\partial C_{pi}}{\partial r} = 0, \quad r = 0 \tag{10}$$

where $D_{api} = D_{pi} + D_{si}(\partial q_i/\partial c_i)$

The mass balance equations for each solute in the given chromatographic system are then coupled by the PIQ isotherm given in Eqs. (1) and (2).

2.3. Numerical method

The spatial discretization of the bulk phase was done using the Galerkin finite element formulation [36]. The approach of the Galerkin finite element method is to solve the system of equations in residual form until the residuals are zero. The differential form of the bulk phase Eq. (4) given above assumes that the solutions variables can be expanded in Taylor's series and therefore are smooth functions with respect to space and time. However, in the presence of sharp discontinuities, the solution lacks the sufficient smoothness requirements, and the differential form cannot be applied. Hence, a more basic form of the equation, the weak form, which decreases the continuity requirements of the solution, was utilized. The dimensionless form of the transport equations and their discretized form are presented in Appendix. The axial dimensionless length is divided into 110 finite elements and piece-wise quadratic shape functions were used to interpolate the solution over each element domain.

For the particle phase transport, the equations were discretized using the orthogonal collocation on finite elements. Lagrange polynomials were used as the trial functions. Orthogonal collocation was applied over each element (maximum number of elements were 3), and the continuity requirement was applied over each intersecting boundary of an element. At the particle boundary (at the center and the surface of a spherical particle), boundary conditions (6–7 and 10–11) were employed. Collocation points used in this work are the roots of the orthogonal Legendre polynomial. The collocation matrices (A and B, Eqs. (29) and (30), respectively) were calculated using the quadrature rule employing a Lagrange polynomial as the trial functions. The formulation chosen for calculation of these matrices preserves the orthogonality of each trial function.

The above discretized particle phase equations were then coupled with the discretized bulk phase equations. The concentration variables were assembled element by element and solved simultaneously using a differential algebraic solver. The element assembly procedure remains the same irrespective of the discretization procedure being used in the axial domain. The detailed analysis is presented in AppendixAppendix A.

The above discretized bulk phase ordinary differential equations were solved simultaneously with the particle phase equations (which are discretized using the orthogonal collocation on finite elements) using the differential algebraic solver DDASPK (Petzold, 1982).

2.4. Moment analysis

The general rate model coupled with the PIQ isotherm under linear adsorption conditions was transformed into the Laplace domain. Subsequently, the variance equations were derived from the first and second moment analysis. The following peak variance equations of protein and displacer as a function of flow rate and salt concentrations were used for the HIC system.

$$\text{Variances} = 2\frac{D_a L}{u_i} + \frac{2Lu_i\varepsilon_p^2 b_0^2\phi^2}{[1+\phi\varepsilon_p b_0]^2} \times \left[\frac{R}{3k_f} + \frac{R^2}{15\phi D_p(1+\varepsilon_p(b_0-1)\varsigma)} + \frac{(b_0-1)^2}{\phi b_0^2 k_{\text{ads}}}\right] \tag{11}$$

$$b_0 - 1 = k' = \frac{1-\varepsilon_p}{\varepsilon_p} a\exp(\alpha + \beta\cdot C_{\text{salt}} + \gamma\cdot\log(C_{\text{salt}})) \tag{12}$$

$$\varsigma = \frac{D_s}{D_p} \tag{13}$$

$$\phi = \frac{1-\varepsilon_0}{\varepsilon_0} \tag{14}$$

where ϕ denotes the phase ratio. Other parameters are the same as defined in the previous section. The interstitial velocity u_i and b_0 are the two operational parameters. Here, b_0 is related to the retention factor of protein and displacer as shown in Eq. (12). From Eqs. (11)–(14), we can estimate the following parameters from the peak variance analysis: the axial dispersion coefficient, D_a; the pore diffusion coefficient, D_p; the surface diffusion coefficient, D_s; the film mass transfer coefficient, k_f; and the adsorption rate constant, k_{ads}.

The axial diffusion is contributed from molecular diffusion and eddy diffusion. The molecular diffusion is negligible for a macromolecular system. Therefore, the axial diffusion coefficient is related to the eddy diffusion by the following equation:

$$D_a = \xi \cdot u \tag{15}$$

where ξ is a proportional factor. Therefore, Eq. (14) can be modified as

$$\text{Variances} = 2\xi L + \frac{2Lu_i\varepsilon_p^2 b_0^2\phi^2}{\left[1+\phi\varepsilon_p b_0\right]^2} \times \left[\frac{R}{3k_f} + \frac{R^2}{15\phi D_p(1+\varepsilon_p(b_0-1)\varsigma)} + \frac{(b_0-1)^2}{\phi b_0^2 k_{ads}}\right] \tag{16}$$

Under the unretained conditions, $b_0 = 1$. Hence, Eq. (16) can be simplified into:

$$\text{Variances} = 2\xi \cdot L + \frac{2L\varepsilon_p^2\phi u_i}{[1+\phi\varepsilon_p]^2}\left[\frac{R}{3k_f} + \frac{R^2}{15\phi\varepsilon_p D_p}\right] \tag{17}$$

Therefore, in the plot of peak variances vs. flow rate, we can estimate the axial diffusion coefficient from the intercept and pore diffusion coefficient from slope. The film transport coefficient can be estimated from a well-established relationship [44]:

$$Sh = 2 + 1.45 \cdot Re^{1/2} \cdot Sc^{1/3} \tag{18}$$

As we can see from Eq. (18), both Schmidt number and Sherwood number are dependent on the molecular diffusion coefficient, D_m. Generally, the D_m is estimated from the Wilke–Chang equation. However, for a system that involves molecules with Mw larger than 1000 (e.g. proteins), we can use the following semi-empirical relationship [45]:

$$D_m(\text{cm}^2\text{S}^{-1}) = 2.74 \times 10^{-5}\ \ \text{M}^{-1/3} \tag{19}$$

where M is the molecular weight.

In addition, the variance obtained from the external tubing was subtracted to obtain accurate solute transport variances in the column.

3. Experimental methods

3.1. Materials

Lysozyme (hen egg white) and lectin (arachis hypogaea, peanut) were purchased from Sigma (St. Louis, MO). Big Chap was purchased from Calbiochem (La Jolla, CA). A size exclusive column (G3000SWXL) with a guard column (SW) was purchased from Tosoh Biosep (Montgomeryville, PA). Phenyl 650M bulk resin was donated by Tosoh Biosep (Montgomeryville, PA). Sodium phosphate (monobasic), sodium phosphate (dibasic), ammonium sulfate, sodium chloride, sodium nitrate and blue dextran (Mw 2,000,000) were purchased from Sigma (St. Louis, MO, USA).

3.2. Apparatus

Analytical scale isocratic experiments were conducted to obtain protein retention profiles in the presence of various ammonium sulfate concentrations. The isocratic experiments were carried out using a chromatographic system from Waters (Milford, MA), which consisted of a 600E Multi-solvent Delivery System, a 484 UV–Vis absorbance detector and a 712 WISP auto sampler with a cooling module.

All analytical scale displacement experiments were conducted on a Model 590 programmable HPLC pump (Waters, Milford, MA) connected to the chromatographic columns via a Model C10W 10-port valve (Valco, Houston, TX). Data acquisition and processing were carried out using a Strawberry Tree system (Sunnyvale, CA). The column effluent was monitored using a Waters 484 UV–Vis absorbance detector (Milford, MA). Fractions of the column effluent were collected using an LKB 2212 HeliFrac fraction collector (LKB, Sweden).

All analytical scale linear gradient experiments were conducted on a fast liquid chromatographic system (FPLC) donated by GE Healthcare (Uppsala, Sweden), which consisted of two P-500 pumps, a liquid chromatography controller LCC-500 Plus and a motor valve MV-7. Data acquisition and processing were carried out using a Strawberry Tree system (Sunnyvale, CA). The column effluent was monitored using a Waters 484 UV–Vis absorbance detector (Milford, MA). Fractions of the column effluent were collected using an LKB 2212 HeliFrac fraction collector (LKB, Sweden).

Analysis of the collected fractions was carried out using a chromatographic system from Waters (Milford, MA), which consisted of a 600E Multi-solvent Delivery System, a PDA 996 photodiode array detector and a 712 WISP auto sampler with a cooling module.

3.3. Frontal experiments to obtain adsorption isotherms of proteins and displacer

A phenyl 650M column (90 mm × 5 mm I.D.) was initially equilibrated with the carrier buffer, 100 mM sodium phosphate (pH 7.0) consisting of various concentrations (700 mM, 900 mM, 1000 mM, 1100 mM and 1350 mM) of ammonium sulfate. The column was then sequentially perfused with proteins or displacer solutions dissolved in the same salt concentration buffer. The column effluent was monitored at 215 nm and the flow rate was 0.2 ml/min. All experiments were carried out at room temperature.

3.4. Determination of column porosity

The total porosity of the HIC column was measured by pulse injection of sodium nitrate in 50 mM phosphate buffer, pH 7.0, containing 20 mM ammonium sulfate. External porosity was determined by pulse injection of blue dextran (average Mw = 2,000,000) in the same buffer. The delay volume of the system, which includes extra-column tubing, void volumes of column fittings and the detector were determined by pulse injections of sodium nitrate with the column off-line. The flow rate was 0.2 ml/min. All experiments were conducted at room temperature.

3.5. Linear gradient chromatography

A phenyl 650M column (90 mm × 5 mm I.D.) was initially equilibrated with the carrier buffer, 100 mM sodium phosphate, pH 7.0, containing 1.1 M ammonium sulfate. A 40-min linear gradient from 1.2 M ammonium sulfate to 0.9 M ammonium sulfate was conducted. 500 μl fractions of the column effluent were collected during the feed loading and linear gradient procedures for subsequent analysis of proteins concentrations. The column effluent was monitored at 215 nm and the flow rate was 0.2 ml/min. The column was regenerated sequentially with five-column volumes of DI water, five-column volumes of regeneration buffer (20% ethanol, 20% acetic acid), followed by five-column volumes of DI water. All experiments were carried out at room temperature.

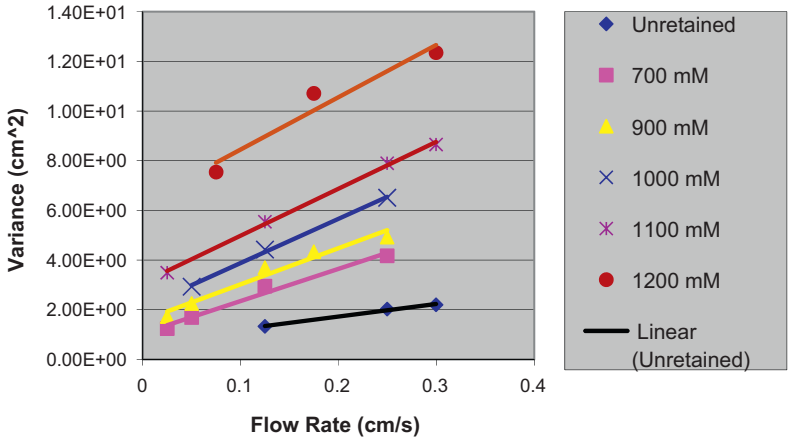

Fig. 1. The peak variances of lysozyme after subtracting extra and film transport contributions as a function of flow rate at different concentrations of salt. (♦) Unretained conditions; (■) 700 mM; (▲) 900 mM; (×) 1000 mM; (✳) 1100 mM; (●) 1200 mM.

3.6. Displacement chromatography

The phenyl 650M column (90 mm × 5 mm I.D.) column was initially equilibrated with the carrier buffer, 100 mM phosphate, pH 7.0, containing 1.35 M ammonium sulfate, for 5 column volumes. The column was then sequentially perfused with the protein feed, displacer and regeneration solutions. The displacer solution of big chap was prepared in 100 mM phosphate buffer, pH 7.0, containing 1.0 or 1.1 M ammonium sulfate. 500 μl fractions of the column effluent were collected during the displacement experiments for subsequent analysis of proteins and displacer. The column effluent was monitored at 215 nm and the flow rate was 0.2 ml/min. The column was regenerated sequentially with five-column volume of DI water, five-column volume of regeneration buffer (20% ethanol, 20% acetic acid) and finally with five-column volume of DI water. All experiments were carried out at room temperature.

3.7. Determination of peak variances

To obtain protein and displacer variances, the phenyl 650M column (90 mm × 5 mm I.D.) was initially equilibrated with the carrier buffer, 100 mM phosphate, pH 7.0, containing various concentrations of ammonium sulfate (0.2, 0.7, 0.9, 1.1 and 1.2 M). A small amount of protein (50 μg) or displacer sample was then injected into the HIC column. The column effluent was monitored at 215 nm wavelengths and different flow rates (0.1, 0.2, 0.5, 0.7, 1.0 and 1.2 ml/min) were used in each set of experiments. All experiments were carried out at room temperature.

The first moment of the elution peaks were used to estimate the b_0 for a particular salt concentration at a particular flow rate. The second moment of the elution peaks were used to estimate the peak variances for the particular condition, and then used in Eq. (16) for parameter estimation.

The original data were exported from the Millenium 2010 workstation. MATLAB was then used to fit the original data to obtain the elution peak first and second moment. Furthermore, the system noise was filtered using the MATLAB function, BUTTER, before calculating the peak second moment.

V'_{column} denotes the variances of the column where film mass transport contributions and extra column contributions have been subtracted from the total variance. V'_{column} was then plotted as a function of velocity at different salt concentrations. Eq. (17) reduces to the following expression once the film contribution is subtracted:

$$\text{Variances} = 2\xi \cdot L + \frac{2L\varepsilon_p^2 \phi u_i}{[1+\phi\varepsilon_p]^2}\left[\frac{R^2}{15\phi\varepsilon_p D_p}\right] \quad (21)$$

From Eq. (22), under unretained conditions, one can estimate the axial diffusion coefficient from the intercept and the pore diffusion

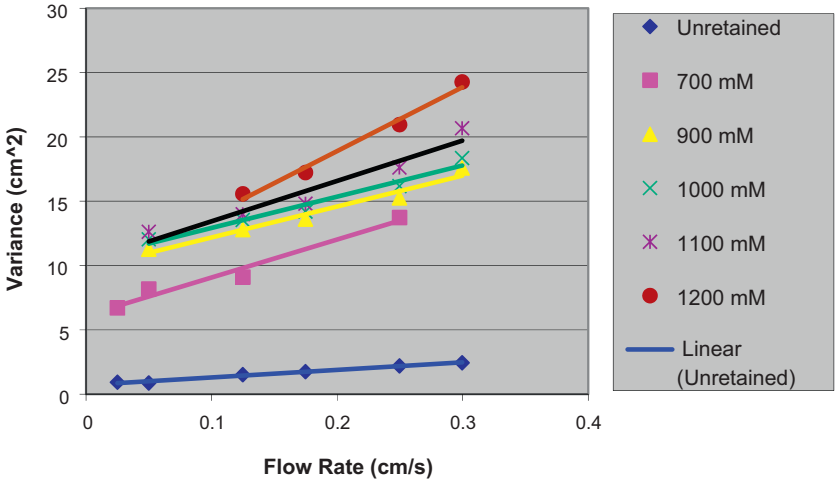

Fig. 2. The peak variances of lectin after subtracting extra and film transport contributions as a function of flow rate at different concentrations of salt. (♦) Unretained conditions; (■) 700 mM; (▲) 900 mM; (×) 1000 mM; (✳) 1100 mM; (●) 1200 mM.

Table 1
PIQ parameters for three model solutes on Phenyl 650M resin.

	Lysozyme	Lectin	Big chap
α	8.16	10.20	2.20
β	0.0071	0.011	0.0037
γ	−2.00	−2.66	−0.36
a	1.43	0.37	0.89
b	0.31	0.13	0.0065
c	1.04	0.23	−2e−04
d	5.21	2.03	−0.021

coefficient from the slope. From Eq. (16), the ς and k_{ads} values can be estimated from the slope obtained under various retention conditions. The MATLAB function, CONSTR, was used to run the global optimization to determine the best fit of the data.

3.8. Protein and displacer analysis by SEC

The effluent fractions in linear gradient and displacement chromatography were analyzed by size exclusive chromatography using a G3000SWXL column from Tosoh Biosep (Montgomeryville, PA). Proteins were monitored at 280 nm and displacer was monitored at 215 nm. The following buffer was used to perform the SEC analysis: 190 mM sodium phosphate, pH 7.6 with 200 mM sodium chloride. The flow rate was 1 ml/min. All experiments were conducted at room temperature.

4. Results and discussions

4.1. Characterization of HIC resin

To enable the characterization of HIC resins, it is essential to identify the transport and kinetic parameters of solutes in these resins. In order to illustrate the resin characterization methodology, the proteins lysozyme HEW (Mw = 14.3 kDa, = 10.5) and lectin (Mw = 40 kDa, pI = 8.5) along with one low molecular mass displacer (big chap, Mw = 878.1) were employed. The resin employed in this work was Phenyl 650M HIC with an average particle size of 65 μm, and a particle size distribution ranging from 40 to 90 μm. This resin contains phenyl functional groups presented on a polymethacrylate polymer backbone. The interstitial and total porosity of the column were estimated as 0.34 and 0.81, respectively, using the techniques described in Section 3.

Table 1 presents the multicomponent PIQ adsorption isotherm [26,28] parameters for the two proteins and the displacer on this HIC system. The detailed method for estimation of these parameters is discussed elsewhere [28]. Briefly, frontal chromatography was carried out to determine the adsorption isotherms for the three model solutes at various ammonium sulfate concentrations. The PIQ parameters were then optimized using the CONSTR optimization functions in Matlab and the corresponding values are presented in Table 1. The parameters α, β and γ obtained by fitting the experimental data to Eq. (2) are given in Table 1. The β and γ values represent the linear and nonlinear regions, respectively, of the $\ln k'$ plot. As seen in the table, the β values are positive for both proteins and displacer. Since $\beta = -(n \cdot \Delta\nu_1/m_1 \cdot g)$, a positive value of β indicates that $\Delta\nu_1$ is negative, thus implying that water molecules are released from the protein and ligand surface during the adsorption process. The γ value represents the release or salt ions during the adsorption process. As seen in Table 1, the γ values are negative for all three solutes, indicating that the local ion concentration around the adsorbed protein is lower than the bulk ion concentration.

The variances (V'_{column}) of the two proteins and the displacer as a function of the linear flow rate under unretained and retained conditions are presented in Figs. 1–3. As seen in the figures, a linear relationship was observed between the variances and the flowrates of the solutes. The data in Figs. 1–3 were used to estimate the transport and kinetic parameters of the three solutes on the HIC resin as described above. The axial diffusivity D_a, the dispersion coefficient ζ, and the pore diffusion coefficient D_p, were computed using Eq. (22) from data under unretained conditions. The surface diffusion coefficient D_s and the adsorption rate constant k_{ads} were computed using Eq. (16) from the global optimization results using CONSTR function (MATLAB) under retained conditions.

Table 2
Summary of the transport parameters obtained from injection of various solutes under retained and unretained conditions.

	Lysozyme	Lectin	Big chap
D_a (m^2/s)	1.129E−10	7.39E−11	1.129E−10
k_f (m/s)	1.29E−05	9.40E−06	1.23E−05
D_p (cm^2/s)	3.61E−07	3.30E−07	3.66E−07
D_s (cm^2/s)	5.72E−07	2.36E−08	6.90E−07
ζ (cm)	5.864E−3	7.05E−3	5.14E−3
k_{ads} (/s)	0.57	0.27	1.02

Table 3
Descriptions of various dimensionless groups.

Dimensionless groups	Descriptions
$N_p = \frac{D_p L}{d_p^2 u}$	$\frac{\text{Pore diffusion}}{\text{Convection}}$
$N_p = \frac{D_p L}{d_p^2 u}$	$\frac{\text{Surface diffusion}}{\text{Convection}}$
$N_s = \frac{D_s L}{d_p^2 u} k'(PIQ)$	$\frac{\text{Film diffusion}}{\text{Convection}}$
$N_{pe} = \frac{uL}{D_a}$	$\frac{\text{Convection}}{\text{Axial dispersion}}$

Eqs. (16) and (17) indicate that the variances vs. velocity plots should have a linear relationship with the same intercept obtained at varying salt concentrations. As can be seen in Figs. 1–3, an increase of the intercept was observed with increasing salt concentration. One possible explanation for this might be that the axial diffusivity decreases with an increase in salt concentration because of the electron shielding at high salt concentration, with a resultant increase in solute diffusion.

The transport and kinetic parameters of the proteins (lectin and lysozyme) and the displacer (big chap) are listed in Table 4. As seen in the table, for both proteins and displacer, pore and surface diffusion play an important role in the phenyl 650M resins. The greatest difference in transport parameters was observed for the kinetic adsorption coefficient between the proteins and the displacer (Table 2). This implies that that the difference in solute transport in the stationary phase is due primarily to the binding kinetics. In addition, as can be seen in the table, while the surface diffusion coefficient of lysozyme was higher than lectin, the pore diffusion coefficients were similar for both the proteins and the displacer. We hypothesize that the size of the proteins (lysozyme, 4 nm; lectin, 7 nm) is responsible for the higher surface diffusion coefficient for lysozyme. The dimensionless groups of these transport parameters were then determined to ascertain the relative importance of the various transport mechanisms. Table 3 describes the various dimensionless groups. The computed dimensionless groups for these three solutes are listed in Table 4 where the lower the value, the more limiting the transport mechanism as compared to convection. As can be seen in the table, both axial dispersion and film mass transport do not play a major limiting role in these systems. In contrast, pore and surface diffusion are generally much slower than the convection, and are potentially rate-limiting steps for solute mass transport in this HIC system. For the proteins, both pore and surface diffusion play a role, while for the displacer, surface diffusion appears to play less of a role.

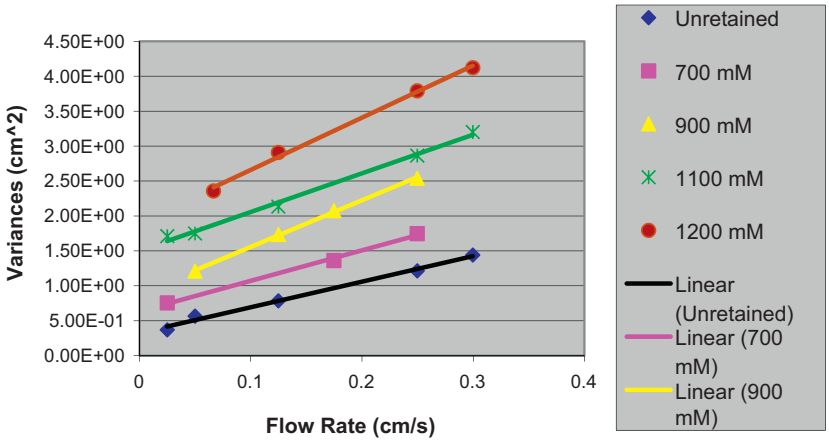

Fig. 3. The peak variances of big chap after subtracting extra and film transport contributions as a function of flow rate at different concentrations of salt. (♦) Unretained conditions; (■) 700 mM; (▲) 900 mM; (✳) 1100 mM; (●) 1200 mM.

Table 4
Summary of the dimensionless groups.

Dimensionless group	Lysozyme	Lectin	Big chap
N_p	0.076/u	0.070/u	0.077/u
N_s	0.087/u	0.017/u	1.31/u
N_f	5.3/u	3.86/u	5.05/u
$1/N_{pe}$	9695	1223	1958

4.2. Model verification of HIC displacement and gradient separations

An ideal displacement separation system (i.e. a system with infinitely fast mass transfer kinetics) will exhibit sharp discontinuities between adjacent zones in the displacement train. However, real HIC displacement systems can have significant transport (e.g. pore and surface diffusion) limitations, which can result in shock layers between the adjacent zones, resulting in loss of purity and yield. The shock layer represents a balance between the thermodynamic self-sharpening effects and the dispersive effects of non-idealities [46].

Since solute transport was strongly affected by both pore and surface diffusion, the general rate model was employed for describing displacement and gradient separations in HIC systems. Figs. 4–6 compare the experimental and simulation results of HIC displacement chromatography and linear gradient chromatography.

Displacement chromatography of the proteins lysozyme and lectin using big chap as the displacer was carried out and the results are given in Figs. 4 and 5 For Fig. 4, the feed load for lysozyme and lectin was 5.7 mg and 3.6 mg, respectively, and the displacer concentration was 8 mM. In Fig. 5, the feed load for lysozyme and lectin was 2.5 mg and 2.5 mg, respectively, and the displacer concentration was 5 mM. The loading conditions for both displacement experiments were 1.2 M salt, and the displacements were then carried out in 1.1 M salt.

In both displacements (Figs. 4 and 5), the displacer is effective at displacing both proteins. Although isotachic square zone profiles are not achieved due to transport limitations, reasonable separation of the proteins occurs. In comparing the two displacements, one can see that the higher displacer concentration used in Fig. 4 results in higher protein concentrations, while the lower displacer concentration used in Fig. 5 resulted in more effective separation. In both displacements, the proteins emerged at higher concentrations than the gradient separation shown in Fig. 6.

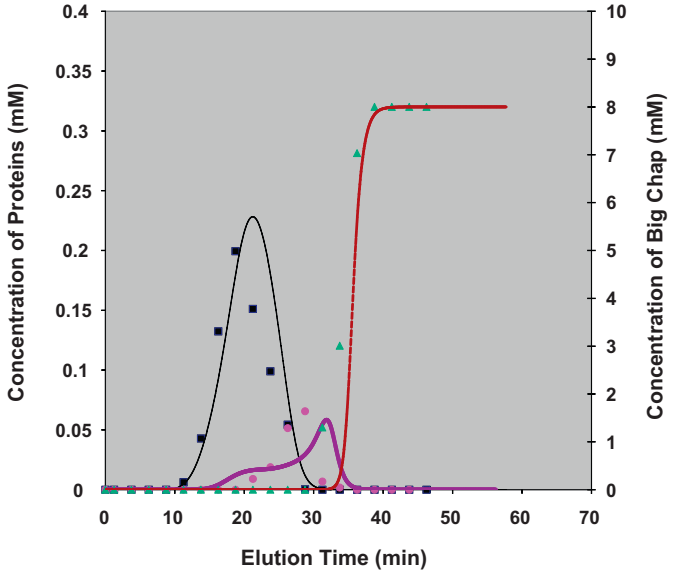

Fig. 4. Modeling of HIC displacement chromatography using general rate model. Mobile phase: 100 mM phosphate buffer at pH 7.4 containing 1100 mM ammonium sulfate. Total loaded 5.7 mg lysozyme and 3.6 mg lectin. Displacer concentration: 8 mM. Column: Tosoh Biosep Phenyl 650M. Column dimension: 95 mm × 5 mm. Flow rate is 0.2 ml/min. Experiment done at room temperature. (■) Lysozyme experiment data; (●) lectin experiment data; (▲) big chap experiment data; (– – –) lysozyme simulation data; (—) lectin simulation data; (. . .) big chap simulation data.

As can be seen from these figures, there was relatively good agreement between the experimental data (symbols) and the simulation results (solid lines). The big chap breakthrough with 5 mM concentration was not as sharp as that obtained with 8 mM, which is to be expected. While the lysozyme and displacer profile were predicted well from the simulations, the lectin had some discrepancies. It is interesting to note that in a previous publication [28], the PIQ isotherm was able to accurately fit the lectin adsorption behavior over a range of conditions. Thus, this slight discrepancy might be due to multicomponent adsorption effects, which will be the subject of a future report.

Fig. 6 compares the experiment and simulated results of lysozyme and lectin separation by linear gradient hydrophobic interaction chromatography. The total loading of lysozyme and lectin is 2.5 mg and 1.6 mg, respectively. Linear gradient separation of model mixture was carried out using a gradient from 1.2 M

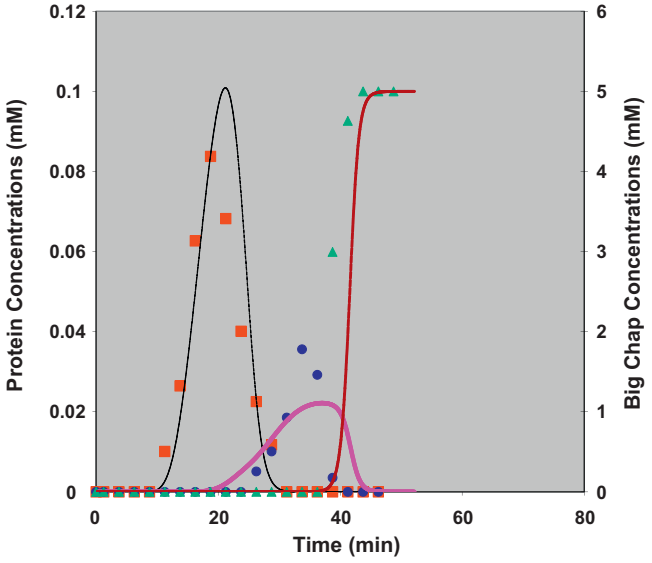

Fig. 5. Modeling of HIC displacement chromatography using general rate model. Mobile phase: 100 mM phosphate buffer at pH 7.4 containing 1100 mM ammonium sulfate. Total loaded 2.5 mg lysozyme and 2.5 mg lectin. Displacer concentration: 5 mM. Column: Tosoh Biosep Phenyl 650M. Column dimension: 95 mm × 5 mm. Flow rate is 0.2 ml/min. Experiment done at room temperature. (■) Lysozyme experiment data; (●) lectin experiment data; (▲) big chap experiment data; (– – –) lysozyme simulation data; (—) lectin simulation data; (. . .) big chap simulation data.

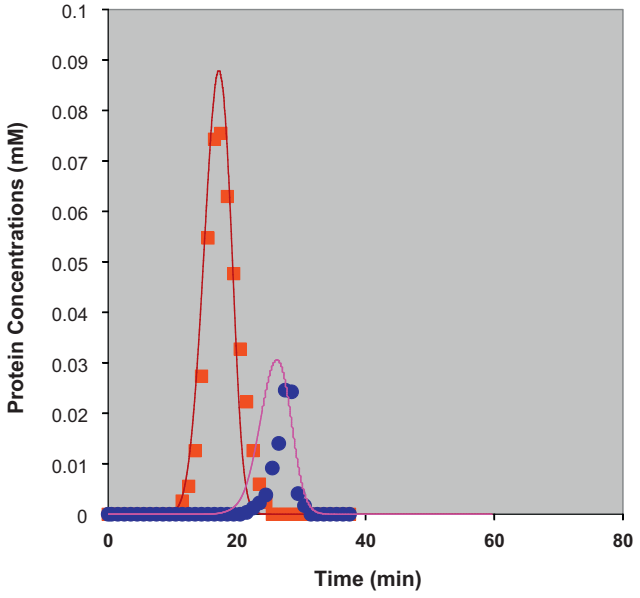

Fig. 6. Modeling of HIC gradient chromatography using general rate model. Mobile phase A: 100 mM phosphate buffer at pH 7.4 containing 1.2 M ammonium sulfate; Mobile phase B: 100 mM phosphate buffer at pH 7.4 containing 0.7 M ammonium sulfate. 100-min linear gradient from 100% buffer A to 100% buffer B. Total loaded 2.5 mg lysozyme and 1.6 mg lectin. Column: Tosoh Biosep Phenyl 650M. Column dimension: 95 mm × 5 mm. Flow rate is 0.2 ml/min. Experiment done at room temperature. (■) Lysozyme experiment data; (●) lectin experiment data; (—) lysozyme simulation data; (– – –) lectin simulation data.

to 0.7 M ammonium sulfate for 100 min. As can be seen from the figure, the experimental results are in good agreement with the simulations; however, there is again a minor discrepancy for lectin, which elutes slightly later than predicted by the theory.

These results with both the displacement and the gradient systems, illustrate that the PIQ isotherm can be employed in concert with the general rate model for predicting the column behavior of non-linear protein HIC systems.

5. Conclusions

The methodology presented in this paper provides a useful tool for the determination of transport parameters and the selection of an appropriate transport model for simulating preparative HIC systems. The results indicate that protein transport in this HIC system was dominated by both pore and surface diffusion. In addition, the simulation results demonstrate the utility of the general rate model coupled with the PIQ isotherm to predict the column behavior of both displacement and linear gradient protein separations. This work sets the stage for future work on the optimization of displacement and gradient preparative HIC separations.

Nomenclature

C_i	concentration of solute in liquid phase
C_{pi}	concentration of solute in pore phase
q_i	concentration of solute in solid phase
u_0	superficial velocity
r	radial distance in pore of stationary phase
D_{ai}	axial diffusivity
ε_i	interstitial porosity
k_{fi}	interfacial film coefficient
D_{pi}	Pore diffusion coefficient
D_{si}	Surface diffusion coefficient
D_{api}	Apparent diffusion coefficient

Appendix A.

A.1. Dimensionless equations

The Eqs. (1)–(11) can be converted into a non-dimensional form using the following dimensionless variables presented in Table 3.

The dimensionless equations for the generalized model are:

$$\frac{\partial C_{bi}}{\partial \tau} = \frac{1}{P_{ei}}\frac{\partial^2 C_{bi}}{\partial z^2} - \frac{\partial C_{bi}}{\partial z} - N_{fi}[C_{bi} - C_{pi}(\xi = 1)] \tag{22}$$

$$\frac{\partial C_{pi}}{\partial \tau} = N_{pi}\nabla_s^2 C_{pi} - \Phi_{ki} Y_{li} \tag{23}$$

The Laplacian $\nabla_s^2 C$ used in Eq. (24) is defined as

$$\nabla_s^2 C = \frac{1}{z^2}\frac{\partial}{\partial}\left(z^2 \frac{\partial C}{\partial z}\right)$$

where subscript s indicates that the domain is spherical.

$$K_i \frac{\partial \theta_i}{\partial \tau} = K_i N_{si} \nabla \theta_i + \Phi_{ki} Y_{li} \tag{24}$$

where subscript n denotes the component.

Boundary conditions:

$$\frac{\partial C_{bi}}{\partial z} = \left\langle \begin{matrix} Pe_i[C_{bi} - C_{fi}] & z = 0 \\ 0 & z = 1 \end{matrix} \right\rangle \tag{25}$$

$$N_{pi}\frac{\partial C_{pi}}{\partial \xi} + K_i N_{si}\frac{\partial \theta_i}{\partial \xi} = \langle Pe_i[C_{pi} - C_{fi}] \quad \xi = 1 \rangle \tag{26}$$

$$2K_i N_{si}\frac{\partial \theta_i}{\partial \xi} = K_i \frac{\partial \theta_i}{\partial \tau} - \Phi_{ki} Y_{li} \quad \xi = 1$$

A.2. Bulk phase discretized equations

To derive the weak form of the above Eq. (23), the differential form is first multiplied by a smooth weighting function W belonging to a space of functions, $W \varepsilon W_h^k$. The resulting product is then integrated over an open space-time domain Ω. Integration by parts then transfers the spatial derivatives from the fluxes on to the weighting function, thus decreasing the continuity requirements of the solution. In turn, boundary integrals appear in the weak form. The weighted residual form of the bulk phase equation can be written as

$$\int_{\Omega^e} W^h \left(\frac{\partial C_{bn}}{\partial \tau} - \frac{1}{P_{en}} \frac{\partial^2 C_{bn}}{\partial z^2} + \frac{\partial C_{bn}}{\partial z} + N_{fn}[C_{bn} - C_{pn}(\xi = 1)] \right) d\Omega^e = 0 \tag{27}$$

where Ω^e is the finite element domain. The integration by parts of the second order differential terms leads to the following weak form:

$$\int_{\Omega^e} W^h C^h_{bn,t} + \frac{1}{P_{en}} + \int_{\Omega^e} W^h_i C^h_{bn,i} d\Omega^e - \frac{1}{P_{en}} W^h C^h_{bn,i}|_{\Gamma^e} + \int_{\Omega^e} (W^h C^h_{bn,i} + N_{fn} W^h C^h_{bn}) d\Omega^e - \int_{\Omega^e} N_{fn} W^h C_{pn}(\xi = 1) d\Omega^e = 0 \tag{29}$$

where C^h_{bn}, W^h are interpolated using shape functions over an element as $C^h_{bn} = \sum_{A=1}^{nnp} N_A C^A_{bn}$, $C^h_{bn,i} = \sum_{A=1}^{nnp} N_{A,i} C^A_{bn}$ and $W^h = \sum_{A=1}^{nnp} N_A D_A$. Since the interpolating functions are chosen to be same for both the solution and the weight space, it leads to a Galerkin form. After substituting C^h_{bn}, W^h with the interpolating functions, a set of nonlinear ordinary differential equations are obtained which in the matrix form can be expressed as:

$$[M_n]\left[C'_{bn}\right] = [K_n][C_{bn}] + [B_n] + [F_n] C_{pn}(\xi = 1) \tag{28}$$

A.3. Particle phase discretized equations

Using orthogonal collocation on finite elements the above equations are discretized for element l and collocation point i as:

$$\frac{dC_{pn,i}}{d\tau} + K_{n,i} \frac{d\theta_{n,i}}{d\tau} = N_{pi} \frac{1}{h_l} \left\{ \sum_{j=1}^{NCOL+2} B_{i,j} C_{pn,j} + \frac{2}{r_l} \sum_{j=1}^{NCOL+2} A_{i,j} C_{pn,j} \right\} + K_n N_{sn,i} \left\{ \sum_{j=1}^{NCOL+2} B_{i,j} \theta_{n,j} + \frac{2}{r_l} \sum_{j=1}^{NCOL+2} A_{i,j} \theta_{n,j} \right\} \tag{29'}$$

For the l-th element,

$$r_l = \frac{\xi - \xi_1}{h_l}, \quad h_l = \xi_{l+1} - \xi_l$$

The discretized boundary conditions for the pore and the solid phase can be represented as

Boundary conditions :

$$N_{\mathrm{pi}} \frac{\partial C_{\mathrm{pi}}}{\partial \xi} + K_i N_{\mathrm{si}} \frac{\partial \theta_i}{\partial \xi} = \left\langle pe_{\mathrm{i}} [C_{\mathrm{pi}} - C_{\mathrm{fi}}] \quad \xi = 1 \right\rangle$$
$$2K_i N_{si} \frac{\partial \theta_i}{\partial \xi} = K_i \frac{\partial \theta_i}{\partial \tau} - \Phi_{\mathrm{ki}} Y_{\mathrm{li}} \quad \xi = 1$$
$$\sum_{j=1}^{NCOL+2} A_{ij} C_{\mathrm{pn,j}} = 0 \left\langle \zeta = 0 \right|$$
$$\sum_{j=1}^{NCOL+2} A_{ij} \theta_{\mathrm{pn,j}} = 0 \left\langle \zeta = 0 \right| \tag{30}$$

References

[1] M.M. Diogo, J.A. Queiroz, G.A. Monteiro, S.A.M. Martins, G.N.M. Ferreira, D.M.F. Prazeres, Biotechnol. Bioeng. 68 (2000) 576.
[2] M.M Diogo, J.A. Queiroz, D.M.F. Prazeres, Bioseparation 10 (2001) 211.
[3] H. Husi, M.D. Walkinshaw, J. Chromatogr. B 736 (1999) 77.
[4] C. Machold, K. Deinhofer, R. Hahn, A. Jungbauer, J. Chromatogr. A 972 (2002) 3.
[5] K.C. O'Connor, S. Ghatak, B.D. Stollar, Anal. Biochem. 278 (2000) 239.
[6] K. Pomazal, C. Prohaska, I. Steffan, J. Chromatogr. A 960 (2002) 143.
[7] K.M. Sunasara, F. Xia, R.S. Gronke, S.M. Cramer, Biotechnol. Bioeng. 82 (2003) 330.
[8] T.T. Jones, E.J. Fernandez, Biotechnol. Bioeng. 87 (2004) 388.
[9] A. Jungbauer, C. Machold, R. Hahn, J. Chromatogr. A 1079 (2005) 221.
[10] T. Tibbs Jones, E.J. Fernandez, J. Colloid Interface Sci. 259 (2003) 27.
[11] R. Ueberbacher, E. Haimer, R. Hahn, A. Jungbauer, J. Chromatogr. A 1198–1199 (2008) 154.
[12] C. Horvath, W. Melander, I. Molnar, J. Chromatogr. 125 (1976) 129.
[13] H.P. Jennissen, Hoppe Seylers Z. Physiol. Chem. 357 (1976) 265.
[14] W. Melander, C. Horvath, Arch. Biochem. Biophys. 183 (1977) 200.
[15] T. Arakawa, S.N. Timasheff, Biochemistry 23 (1984) 5912.
[16] B.F. Roettger, J.A. Myers, M.R. Ladisch, F.E. Regnier, Biotechnol. Progr. 5 (1989) 79.
[17] X.D. Geng, L.A. Guo, J.H. Chang, J. Chromatogr. 507 (1990) 1.
[18] T.W. Perkins, D.S. Mak, T.W. Root, E.N. Lightfoot, J. Chromatogr. A 766 (1997) 1.
[19] F.Y. Lin, W.Y. Chen, M.T.W. Hearn, J. Mol. Recognit. 15 (2002) 55.
[20] M.A.J. Chowdhury, R.I. Boysen, H. Ihara, M.T.W. Hearn, J. Phys. Chem. B 106 (2002) 11936.
[21] W.R. Melander, D. Corradini, C. Horvath, J. Chromatogr. 317 (1984) 67.
[22] W.R. Melander, Z.E. Rassi, C. Horvath, J. Chromatogr. 469 (1989) 3.
[23] J.L. Fausnaugh, F.E. Regnier, J. Chromatogr. 359 (1986) 131.
[24] F. Xia, D. Nagrath, S.M. Cramer, J. Chromatogr. A 1079 (2005) 229.
[25] F. Xia, D. Nagrath, S.M. Cramer, J. Chromatogr. A 989 (2003) 47.
[26] F. Xia, D. Nagrath, S. Garde, S.M. Cramer, Biotechnol. Bioeng. 87 (2004) 354.
[27] R. Ueberbacher, A. Rodler, R. Hahn, A. Jungbauer, J. Chromatogr. A 1217 (2010) 184.
[28] F. Xia, D. Nagrath, S.M. Cramer, J. Chromatogr. 989 (2003) 47.
[29] R.W. Deitcher, J.E. Rome, P.A. Gildea, J.P. O'Connell, E.J. Fernandez, J. Chromatogr. A 1217 (2010) 199.
[30] R.W. Deitcher, Y. Xiao, J.P. O'Connell, E.J. Fernandez, Biotechnol. Bioeng. 102 (2009) 1416.
[31] M.E. Lienqueo, C. Shene, J. Asenjo, J. Mol. Recognit. 22 (2009) 110.
[32] E. Kucera, J. Chromatogr. 19 (1965) 237.
[33] R.G. Luo, J.T. Hsu, Ind. Eng. Chem. Res. 36 (1997) 444.
[34] J.A. Berninger, R.D. Whitley, X. Zhang, N.H.L. Wang, Comput. Chem. Eng. 15 (1991) 749.
[35] Z. Ma, R.D. Whitley, N.H.L. Wang, AlChE J. 42 (1996) 1244.
[36] T. Gu, T.J. Gow, G.T. Tsao, AlChE J. 36 (1991) 784.
[37] M.V. Ernest, R.D.J. Whitley, Z. Ma, N.-H.L. Wang, Ind. Eng. Chem. Res. 36 (1997) 212.
[38] D. Nagrath, A. Messac, B.W. Bequette, S.M. Cramer, Biotechnol. Prog. 20 (2004) 162.
[39] R.D. Whitley, K.E. Vancott, N.H.L. Wang, Ind. Eng. Chem. Res. 32 (1993) 149.
[40] C.K. Lee, Q.M. Yu, S.U. Kim, N.H.L. Wang, J. Chromatogr. 484 (1989) 29.
[41] J. Mollerup, E. Hansen, J. Chromatogr. A 827 (1998) 235.
[42] M.A. Fernandez, G. Carta, J. Chromatogr. A 746 (1996) 169.
[43] V. Natarajan, S. Cramer, Sep. Sci. Technol. 35 (2000) 1719.
[44] S.C. Foo, R.G. Rice, AlChE J. 21 (1975) 1149.
[45] A. Polson, J. Phys. Colloid Chem. 54 (1950) 649.
[46] F.G. Helfferich, P.W. Carr, J. Chromatogr. 629 (1993) 97.